

■ 原著論文 / ORIGINAL PAPER ■

Numerical Simulation of Supersonic Combustion Using Unstructured Point Implicit Finite Volume Method

DEEPU, Mukundan N.^{1*}, GOKHALE, Sadanand. S.², and JAYARAJ, Simon³¹ Dept. of Mechanical Engineering, NSS College of Engineering, Palakkad-678 008, India.² Dept. of Aerospace Engineering, Indian Institute of Technology Madras-600 036, India.³ Dept. of Mechanical Engineering, National Institute of Technology Calicut-673 601, India.

Received 5, July, 2005; Accepted 19, January 2006

Abstract : Numerical simulation of supersonic combustion of hydrogen in air has been done using point implicit finite volume method. This method treats all chemical species terms implicitly and all other terms explicitly. Solver is based on the solution of unsteady, compressible, turbulent Navier-Stokes equations, using Unstructured Finite Volume Method (UFVM) incorporating RNG based κ - ϵ two equation model and time integration using three stage Runge-Kutta method. Reaction of hydrogen with air is modeled using an eight-step reaction mechanism. The preconditioning has found to be effective in overcoming the stiffness in chemically reacting flows. The method is validated against standard experiments for CFD code validation. The predicted values of temperature and species production were in good agreement with experimental results. The code is used to simulate the combustion of hydrogen injected to the wake region formed by a wedge shaped strut.

Key Words : Supersonic combustion, Stiffness, Point implicit method, FVM

1. Introduction

Supersonic Combustion Ramjet engine (SCRAMJET) benefits from the better performance of air breathing propulsion system. Scramjets need a combustor that should have efficient mixing and combustion of fuel with air at supersonic speeds without much pressure loss. Many experimental and numerical analyses [1-3] have been reported during the last few decades regarding the characteristics of the complex flow field resulting due to fuel air mixing and combustion. The use of supersonic combustors in such vehicles requires efficient supersonic combustion within combustor lengths, short enough to be compatible with practical engine sizes. Micro scale mixing is essential as it promotes rapid reaction. Hydrogen has proven its role as fuel in such applications. The present work is an attempt towards the accurate prediction of heat release and species production in Hydrogen-Air mixing layers.

The developed solver is based on two-dimensional Navier Stokes equation governing compressible turbulent flows. The time integration is done using three stage Runge-Kutta method. For modeling Hydrogen-Air reaction, an eight-step reaction

mechanism proposed by Evans and Schexnayder [4] has been used. Flows involving finite rate chemistry are often found to be stiff, hence it is very difficult to solve them numerically using simple explicit methods. The point implicit method suggested by Bussing and Murman [5] is based on the implicit treatment of the chemical species in the source term and is effective in dealing the phenomena with differing time scales simultaneously. The implicit treatment of the chemical species in the source term reduces the stiffness considerably and higher CFL almost equal to that of non-reacting situations has been obtained. Comparison of the numerical result has been done with the standard experimental data for CFD code validation. In the present work hydrogen wall jet experiments of Burrows and Kurkov [6] and axisymmetric reacting free shear flow experimental measurements of Cheng et al. [7] are used. The predicted heat release and species production rates are found to have reasonable agreement with the experimental results. Combustion of hydrogen injected to the wake region formed by a wedge shaped strut has been simulated using the present code.

2. Governing Equations

Navier-Stokes equation for an axisymmetric flow can be

* Corresponding author. Email:- m.deepu@rediffmail.com

written as

$$\frac{\partial U}{\partial t} + \frac{\partial F}{\partial x} + \frac{1}{r} \frac{\partial(rG)}{\partial r} = S \tag{1}$$

Where

$$U = \begin{bmatrix} \rho \\ \rho u \\ \rho v \\ \rho E \\ \rho \kappa \\ \rho \varepsilon \\ \rho Y_i \end{bmatrix}, F = \begin{bmatrix} \rho u \\ \rho u^2 + \sigma_{xx} \\ \rho uv + \sigma_{xr} \\ (\rho E + \sigma_{xx})u + \sigma_{xr}v - K \frac{\partial T}{\partial x} \\ \rho u \kappa - \mu_\kappa \frac{\partial \kappa}{\partial x} \\ \rho u \varepsilon - \mu_\varepsilon \frac{\partial \varepsilon}{\partial x} \\ \rho u Y_i \end{bmatrix}$$

$$G = \begin{bmatrix} \rho v \\ \rho uv + \sigma_{rx} \\ \rho v^2 + \sigma_{xr} \\ (\rho E + \sigma_{rr})v + \sigma_{rx}u - K \frac{\partial T}{\partial r} \\ \rho v \kappa - \mu_\kappa \frac{\partial \kappa}{\partial r} \\ \rho v \varepsilon - \mu_\varepsilon \frac{\partial \varepsilon}{\partial r} \\ \rho v Y_i \end{bmatrix}, S = \begin{bmatrix} 0 \\ 0 \\ 0 \\ \frac{1}{r}(P + \sigma_{\theta\theta}) \\ H_\kappa \\ H_\varepsilon \\ \omega \end{bmatrix}$$

For the present analysis modified κ - ε model called Renormalisation Group (RNG) model was used. Yakhot et al [8] proposed this model, which systematically removes all the small scales of turbulence motion from the governing equation by expressing their effects in terms of large scales and a modified viscosity.

$$\frac{\partial(\rho \kappa)}{\partial t} + \nabla \cdot (\rho \kappa u) = \text{div}[\alpha_\kappa \mu_{\text{eff}} \text{grad} \kappa] + H_\kappa \tag{2}$$

$$\frac{\partial(\rho \varepsilon)}{\partial t} + \text{div}(\rho \varepsilon U) = \text{div}[\alpha_\varepsilon \mu_{\text{eff}} \text{grad} \varepsilon] + H_\varepsilon \tag{3}$$

Here the turbulence source terms are defined as

$$H_\kappa = 2\mu_t E_{ij} - \rho \varepsilon \text{ and } H_\varepsilon = C_{1\varepsilon}^* \frac{\varepsilon}{\kappa} 2\mu_t E_{ij} \cdot E_{ij} - C_{2\varepsilon} \rho \frac{\varepsilon^2}{\kappa}$$

Turbulent viscosity is defined as

$$\mu_t = \rho C_\mu \frac{\kappa^2}{\varepsilon} \tag{4}$$

Closure coefficients are evaluated as

$$C_\mu = 0.0845, \alpha_\kappa = \alpha_\varepsilon = 1.39, C_{1\varepsilon} = 1.42, C_{2\varepsilon} = 1.68$$

$$\eta = \sqrt{(2E_{ij} \cdot E_{ij})^{\kappa/\varepsilon}}$$

$$\text{and } C_{1\varepsilon}^* = C_{1\varepsilon} - \frac{\eta(1 - \eta/\eta_0)}{1 + \beta\eta^3}$$

$$\eta_0 = 4.377, \beta = 0.012$$

Value of constant β is adjustable which is found from near wall turbulence data. All other parameters are explicitly computed as part of RNG process.

For modeling Hydrogen-Air reaction, an eight-step reaction mechanism proposed by Evans and Schexnayder [4] has been used for which the reaction steps and reaction rates are summarised in Table 1. From the law of mass action applicable for any chemical reaction

$$\sum_{i=1}^N \gamma'_{ji} C_i \longleftrightarrow \sum_{i=1}^N \gamma''_{ji} C_i$$

$$(\dot{C}_i)_j = (\gamma''_{ji} - \gamma'_{ji}) \left[k_{f_j} \prod_{i=1}^N C_i^{\gamma'_{ji}} - k_{b_j} \prod_{i=1}^N C_i^{\gamma''_{ji}} \right] \tag{5}$$

Where $i=1,2,3 \dots$ represents species and $j=1,2,3 \dots$ represents reactions

Net change in concentration of any species can be found as

Table 1 Reaction steps and reaction rates

Reaction	Forward Rates			Backward Rates		
	A	N	E	A	N	E
H ₂ +M=H+H+M	5.5×10 ¹⁸	-1.0	51987.0	1.8×10 ¹⁸	-1.0	0.0
O ₂ +M=O+O+M	7.2×10 ¹⁸	-1.0	59340.0	4.0×10 ¹⁷	-1.0	0.0
H ₂ O+M=H+OH+M	5.2×10 ²¹	-1.5	59386.0	4.4×10 ²⁰	-1.5	0.0
OH+M=O+H+M	8.5×10 ¹⁸	-1.0	50830.0	7.1×10 ¹⁸	-1.0	0.0
H ₂ O+O=OH+OH	5.8×10 ¹³	0.0	9059.0	5.3×10 ¹²	0.0	503.0
H ₂ O+H=OH+H ₂	8.4×10 ¹³	0.0	10116.0	2.0×10 ¹³	0.0	2600.0
O ₂ +H=OH+O	2.2×10 ¹⁴	0.0	8455.0	1.5×10 ¹³	0.0	0.0
H ₂ +O=OH+H	7.5×10 ¹³	0.0	5586.0	3.0×10 ¹³	0.0	4429.0

Here M is a third body. The reaction rates are expressed in Arrhenius law form. Units of pre exponent A are multiple of cm³ mole⁻¹ s⁻¹. and that of activation energy E is in Joules

$$\dot{C}_i = \sum_{j=1}^{N_R} \left(\dot{C}_i \right)_j \quad (6)$$

And the net production of species is given by

$$\dot{\omega}_i = \dot{C}_i W_i \quad (7)$$

W_i represents molecular weight of a species.

Reaction rates in the above equation can be found from Arrhenius law

$$k_{fj} = A_j T^{N_j} e^{-\left(\frac{E_j}{RT}\right)}$$

$$k_{bj} = \frac{k_{fj}}{k_{eqj}} \quad (8)$$

Here k_{eqj} is the equilibrium reaction rate.

Evaluation of thermodynamic properties specific heat at constant pressure, enthalpy and entropy are respectively found from standard thermodynamic data from McBride et al [9] as.

$$\frac{C_{p,i}}{R} = A_i + B_i T + C_i T^2 + D_i T^3 + E_i T^4 \quad (9)$$

$$\frac{H_i}{RT} = A_i + \frac{B_i}{2} T + \frac{C_i}{3} T^2 + \frac{D_i}{4} T^3 + \frac{E_i}{5} T^4 + \frac{F_i}{T} \quad (10)$$

$$\frac{S_i}{R} = A_i \times \ln T + B_i T + \frac{C_i}{2} T^2 + \frac{D_i}{3} T^3 + \frac{E_i}{4} T^4 + G_i \quad (11)$$

For each species two sets of coefficients are used for the temperature intervals, one applicable from 300K up to 1000K and the other applicable from 1000K up to 3000K. Total energy of flow field is given by

$$E = \sum_{i=1}^{N_i} Y_i h_i - \frac{p}{\rho} + \frac{1}{2} (u^2 + v^2) \quad (12)$$

Temperature is worked out from the above equation using the Newton-Raphson method. From the modified energy equation, the pressure is calculated from the resulting temperature as follows

$$p = \rho R \sum_{i=1}^{N_i} \frac{Y_i T}{W_i} \quad (13)$$

3. Numerical Method

Basically finite volume technique is an integration of conservation laws. In other words, mass, momentum and energy should be conserved at the basic discrete level. The conservation equation applicable for a cell is

$$\frac{\partial U}{\partial t} + \nabla \cdot F - S = 0 \quad (14)$$

$$\frac{dU_i}{dt} V_i + \sum_{faces} F \cdot ds - S_i \cdot V_i = 0 \quad (15)$$

V_i is the cell volume and ds is the area of elemental sides.

This is a system of ordinary differential equation. For obtaining the solution this has to be integrated with respect to time. The cell averages of the derivative of different flow variables for the surface described by a quadrilateral ABCD can be evaluated as follows.

The derivatives are

$$\left(\frac{\partial U}{\partial x} \right)_{ABCD} = \frac{(U_A - U_C)(y_B - y_D) - (U_B - U_D)(y_A - y_C)}{(x_A - x_C)(y_B - y_D) - (x_B - x_D)(y_A - y_C)}$$

$$\left(\frac{\partial U}{\partial r} \right)_{ABCD} = \frac{(x_A - x_C)(U_B - U_D) - (x_B - x_D)(U_A - U_C)}{(x_A - x_C)(y_B - y_D) - (x_B - x_D)(y_A - y_C)}$$

The surface area is obtained as

$$\int_{ABCD} = \frac{1}{2} [(x_C - x_A)(y_D - y_B) - (x_D - x_B)(y_C - y_A)]$$

A method of successive iteration is used to integrate the governing equation. The variables are updated after each sweep of computational domain. The method is only conditionally stable as it is an explicit method.

For the present analysis the numerical dissipation terms are formed with Laplacian and Biharmonic operators. The dissipation can be written as

$$D(U_i) = d^{(2)}(U_i) + d^{(4)}(U_i) \quad (16)$$

Laplacian operator for the i^{th} cell is given by

$$\nabla^2 U_i = \sum_{k=1}^n (U_k - U_i) \quad (17)$$

where the summation in k is taken over all control volumes which have common "n" interface with the i^{th} cell.

The Biharmonic operator is given by

$$d^{(4)}(U_i) = \sum_{k=1}^n \varepsilon_{ik}^{(4)} \frac{1}{2} \left(\frac{V_i}{\Delta t_i} + \frac{V_k}{\Delta t_k} \right) (\nabla^2 U_k - \nabla^2 U_i) \quad (18)$$

In the above equation

$$\varepsilon_{ik}^{(4)} = \max(0, (k^{(4)} - \varepsilon_{ik}^{(2)}))$$

$k^{(4)}$ values ranges from 1/256 to 3/256 and $k^{(2)}$ values ranges from 0.25 to 0.5.

The artificial Laplacian operator to capture oscillations near shock waves is computed as

$$d^{(2)}(U_i) = \sum_{k=1}^n \varepsilon_{ik}^{(2)} \frac{1}{2} \left(\frac{V_i}{\Delta t_i} + \frac{V_k}{\Delta t_k} \right) (U_k - U_i) \quad (19)$$

Where $\varepsilon_{ik}^{(2)} = k^{(2)} \max(V_i, V_k)$

V_i is a scaling factor given by the undivided Laplacian pressure given by

$$V_i = \frac{\sum_{k=1}^n (p_k - p_i)}{\sum_{k=1}^n (p_k - p_i)}$$

The Biharmonic operator is not operated near shocks as it will produce pre and post shock oscillations.

With the addition of artificial dissipation terms the space discretisation will become

$$V_i \frac{d(U_i)}{dt} + R(U_i) - D(U_i) \tag{20}$$

For the simple explicit scheme the time stepping using Runge-Kutta method can be described as

$$\begin{aligned} U_i^{(0)} &= U_i^{(n)} \\ U_i^{(1)} &= U_i^{(0)} - \alpha_1 \frac{\Delta t_i}{V_i} (R_i^{(0)} - D_i^{(0)}) \\ U_i^{(2)} &= U_i^{(0)} - \alpha_2 \frac{\Delta t_i}{V_i} (R_i^{(1)} - D_i^{(0)}) \\ U_i^{(3)} &= U_i^{(0)} - \alpha_3 \frac{\Delta t_i}{V_i} (R_i^{(2)} - D_i^{(0)}) \\ U_i^{n+1} &= U_i^n + U_i^{(3)} \\ \alpha_1 &= 0.6, \alpha_2 = 0.6 \text{ and } \alpha_3 = 1.0 \end{aligned} \tag{21}$$

Governing equations of turbulent shear layer flows involving finite rate chemistry are often difficult to solve due to stiffness (Ratio of largest time scale to smallest). Stiffness will degrade the performance of numerical methods. While handling two phenomena of differing time scales together, both can be advanced equally in pseudo time. In other words, it can be treated as way of rescaling the equation in time such that both phenomena evolve at comparable pseudo time scales. Then fast process will not hold the slower process. Thereby higher time steps can be achieved. Thus the modified equation is

$$SJ \frac{\partial U}{\partial t} + \frac{\partial F}{\partial x} + \frac{1}{r} \frac{\partial (rG)}{\partial r} = S \tag{22}$$

The point implicit formulation of the time stepping can be written as

$$\begin{aligned} \overline{U_i^{(0)}} &= \overline{U_i^{(n)}} \\ \overline{SJ^0 (U_i^{(1)} - U_i^{(0)})} &= -\alpha_1 \frac{\Delta t_i}{V_i} (\overline{R_i^{(0)}} - \overline{D_i^{(0)}}) \\ \overline{SJ^1 (U_i^{(2)} - U_i^{(0)})} &= -\alpha_2 \frac{\Delta t_i}{V_i} (\overline{R_i^{(1)}} - \overline{D_i^{(0)}}) \\ \overline{SJ^3 (U_i^{(3)} - U_i^{(0)})} &= -\alpha_3 \frac{\Delta t_i}{V_i} (\overline{R_i^{(3)}} - \overline{D_i^{(0)}}) \\ \overline{U_i^{n+1}} &= \overline{U_i^n} + \overline{U_i^{(3)}} \\ \alpha_1 &= 0.6, \alpha_2 = 0.6 \text{ and } \alpha_3 = 1.0 \end{aligned} \tag{23}$$

The point implicit scheme in which all the six chemical

species (H_2, O_2, OH, H, O and H_2O) terms are treated implicitly and all other terms explicitly. The preconditioning [5] Matrix SJ used for this purpose is given by.

$$SJ = \begin{bmatrix} 1 - \alpha_1 \Delta t \frac{\partial \omega_{H_2}}{\partial Y_{H_2}} & -\alpha_1 \Delta t \frac{\partial \omega_{H_2}}{\partial Y_{O_2}} & \dots & -\alpha_1 \Delta t \frac{\partial \omega_{H_2}}{\partial Y_{H_2O}} \\ -\alpha_1 \Delta t \frac{\partial \omega_{O_2}}{\partial Y_{H_2}} & 1 - \alpha_1 \Delta t \frac{\partial \omega_{O_2}}{\partial Y_{O_2}} & \dots & -\alpha_1 \Delta t \frac{\partial \omega_{O_2}}{\partial Y_{H_2O}} \\ \dots & \dots & \dots & \dots \\ -\alpha_1 \Delta t \frac{\partial \omega_{H_2O}}{\partial Y_{H_2}} & -\alpha_1 \Delta t \frac{\partial \omega_{H_2O}}{\partial Y_{O_2}} & \dots & 1 - \alpha_1 \Delta t \frac{\partial \omega_{H_2O}}{\partial Y_{H_2O}} \end{bmatrix} \tag{24}$$

4. Results and Discussion

4.1 Hydrogen Wall Attached Jet Issuing to Hot Vitiated Air Stream

The prediction capability of the code for chemical reaction in supersonic flow field is analysed using a validation test data obtained from Burrows and Kurkov experiment [6]. This experiment has been widely used for code validation. A sonic stream of hydrogen is injected to hot vitiated air stream along a slightly angled down wall. The schematic of the set up is shown in Figure 1. The flow field conditions are summarized in Table 2.

The left face of the computational domain is given with a supersonic inflow condition in the region of supersonic air stream. Hydrogen jet with above-mentioned conditions is introduced at respective position as separate boundary condition. Bottom is a no slip wall and the top face is a free slip wall. A supersonic out flow condition is maintained at outlet. The computational domain was divided into 74000 control volumes with clustering near wall region (edge length of the element in y direction is 0.01 mm). The introduction of point implicit technique has found to be effective in dealing chemical source terms. CFL almost equal to that of compressible turbulent flow (without reaction) could successfully demonstrate this

Table 2 Test conditions in Burrows and Kurkov [6] experiment

Free Stream Conditions	H ₂ Jet	Vitiated Air Stream
Mach Number	1.0	2.44
Temperature, K	254.0	1270.0
Pressure, Pa	101325	101325
H ₂ Mass Fraction	1.0	0
H ₂ O Mass Fraction	0	0.256
O ₂ Mass Fraction	0	0.258
N ₂ Mass Fraction	0	0.486

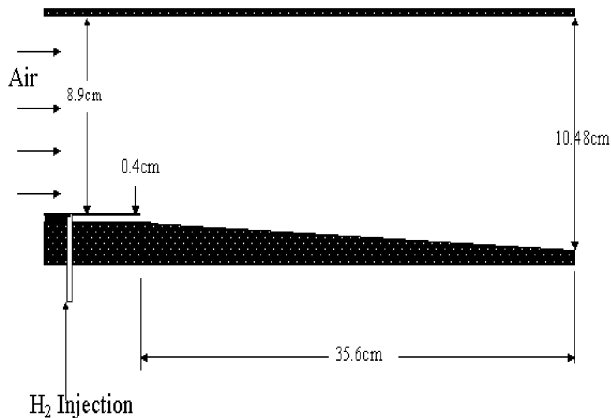


Fig.1 Experimental setup of Burrows and Kurkov [6]

phenomenon.

A detailed comparison of the computed results with experimental data is shown in Figure 2. The RNG turbulence model used in the present analysis could accurately follow the turbulence chemistry interaction. The predicted variations of species mole fractions were in good agreement with experimental data. The non-reacting hydrogen diffuses down along the wall and the reaction is confined in the mixing layer. The enlarged view of the reaction zone is shown in Figure 3.

Once reaction is initiated, much alteration in the predicted values of species concentration and temperature are not observed because the reaction is confined to the low velocity region of the flow field. The OH mole fraction is less by an order compared to that of water as its production is of highly fluctuating in nature and is unstable. The average non-reacting hydrogen concentration is decreasing along the wall and it causes a small decrease in temperature and did not overcome by increase in mixing and reaction. The flame spreads upwards as it move along the wall.

4.2 Coaxial Hydrogen-Air Supersonic Mixing and Reaction

Numerical simulations were performed on an axisymmetric configuration consisting of coaxial jets (Hydrogen and vitiated air) exiting at supersonic velocities into ambient air. Cheng *et al.* [7] made measurements for of temperature and composition have been carried out using ultra-violet Raman scattering and laser induced pre-dissociative fluorescence techniques and an exhaustive set of data are available for validation. The flow conditions have been summarized in Table 3. The details of computational domain are given in Fig. 4. The left face of the computational domain is given with a supersonic inflow condition in the region of supersonic air stream. The burner lips were assumed to non-catalytic. This experiment has been numerically analysed by Baurle *et al.* [10]. Hydrogen jet with

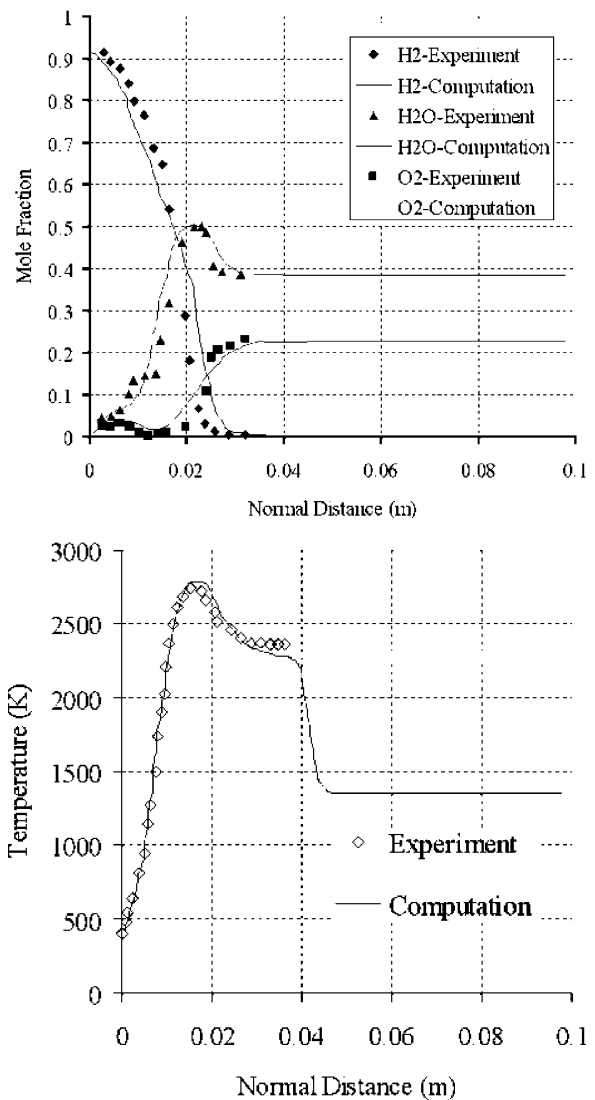


Fig.2 Comparison of computed results with experimental data (a) Species mole fraction profiles at exit plane. (b) Temperature profile at exit plane.

above-mentioned conditions is introduced at respective position as separate boundary condition. Remaining portion in left face is considered as no slip wall. Top face is a no slip wall. A supersonic out flow condition is maintained at outlet. Since the entire flow field is symmetrical about axis of the coaxial jet, a symmetry condition is utilized there. The computational domain was discretised in to 104000 control volumes. The entire domain is initialized with ambient conditions. The grid was added to allow specification of the entrainment boundary condition well upstream of the coaxial jets. The grid is clustered to give more resolution near the lip regions in the transverse direction, and near the burner exit in the streamwise direction.

The introduction of point implicit technique has found to be effective in dealing chemical source terms. CFL almost equal to that of compressible turbulent flow (without reaction) could

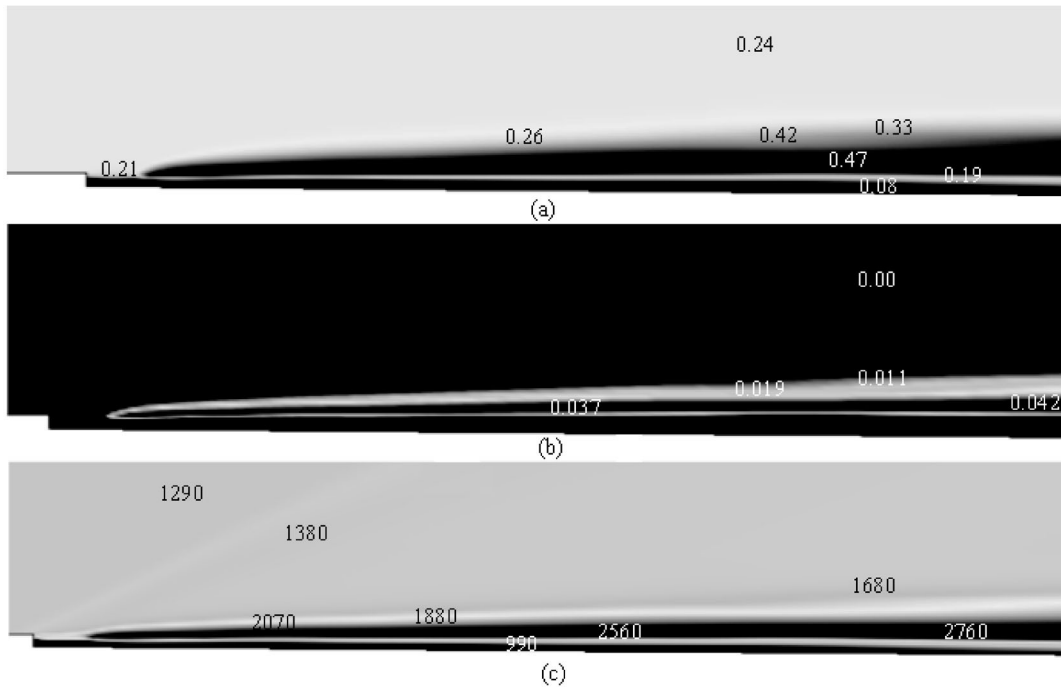


Fig.3 Field view of the computed results in the reaction zone of the flow field (a)Water mole fraction, (b) OH mole fraction and (c) Temperature

Table 3 Coaxial burner exit conditions

	H ₂ Jet	Air Jet	Ambient
Diameter (mm)	2.36	17.8	120
Mach Number	1.0	2.0	0
Pressure (MPa)	0.112	0.107	0.101
Temperature (K)	545	1250	300
Y _{H2}	1.0	0.0	0.0
Y _{O2}	0.0	0.24	0.23
Y _{H2O}	0.0	0.175	0.01

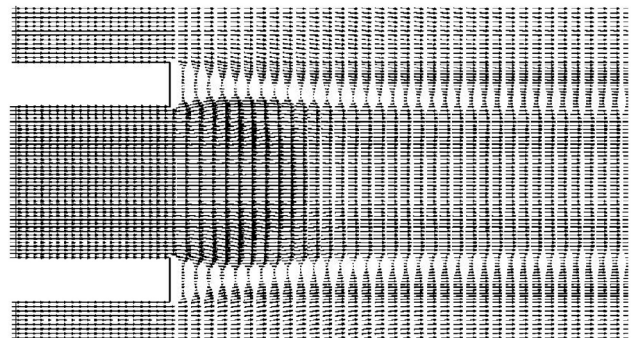


Fig.5 Velocity vectors near jet outlets

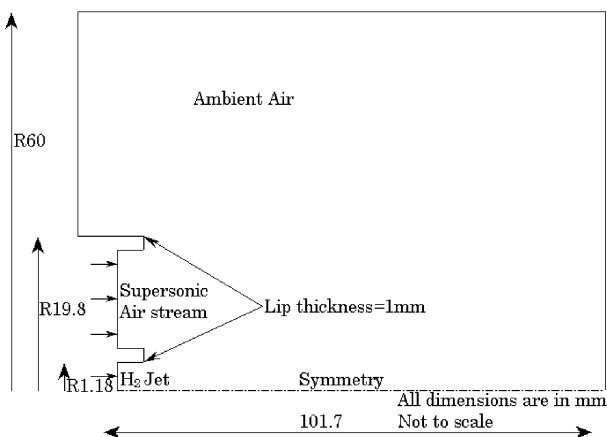


Fig.4 Details of computational domain

successfully demonstrate this phenomenon. Vector plot for the mixing region near jet outlets is shown in Fig. 5. Low velocity regions can be found in mixing layer with recirculations near lip region, this leads to enhanced mixing of the jets. The lip height has a significant role in deciding the nature of recirculation region around it.

Among an exhaustive set of data, a selective set of result of the comparison of the predicted value of temperature at exit of the computational domain ($X/D=43.1$ or 101mm from jet outlet) with experiment is shown in Fig. 6. Reasonable match has been obtained inside core region of the jet and a slight difference in the mixing layers. The difference is due to the value of initial turbulence level given at the inlet and also due to the numerical dissipation effects.

The Mach field view for the mixing layers near to the jet outlet

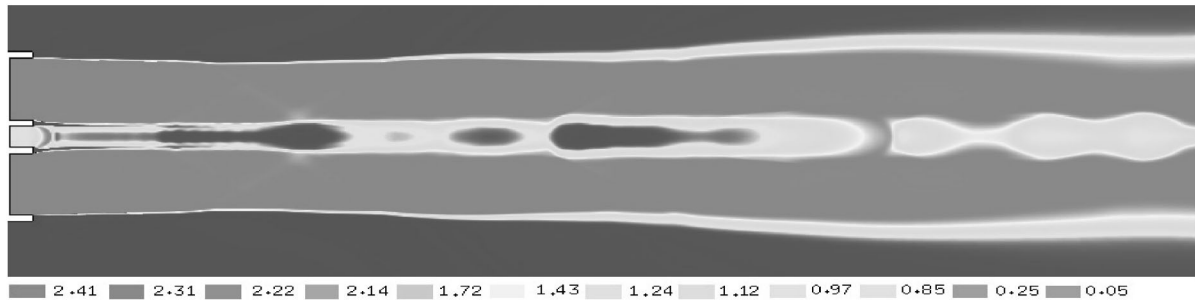


Fig.6 Mach field view for the mixing region

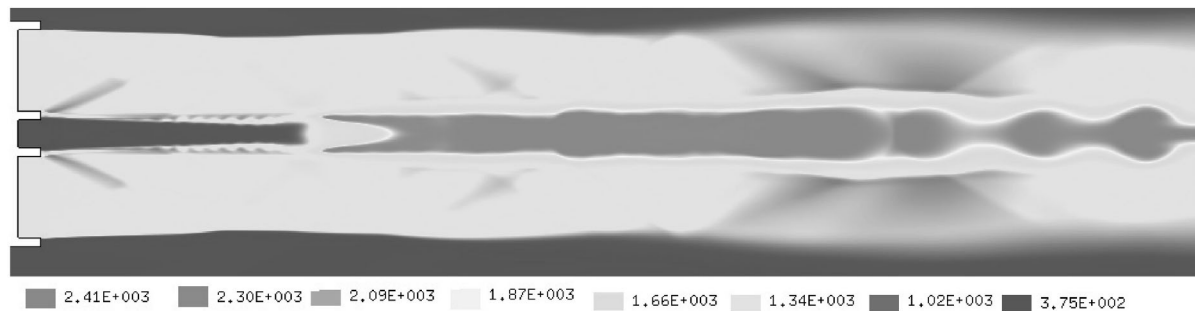


Fig.7 Field view of temperature for the entire domain

is shown in Fig. 6. Alternate compression and expansion takes place for the jet and is not enough to perturb the flow field much in the region near to the jet outlets. The thickness in the lip region, separating the two flows, creates small expansions that are further suppressed by latter stream. The alternate compression-expansion wave patterns found getting gradually weakened due heat release and viscous effects in the region. The temperature plot for the entire domain is given in Fig. 7. The mixing becomes more predominant in the region far from the jet outlets and heat release gradually increases in the mixing layer between hydrogen and air. Non-reacting fuel core extends up to 30mm from jet outlets. Outer layer between supersonic air stream and ambient has almost same temperature through out the length, beyond this non reacting core region.

Comparison of predicted OH mole fraction profiles with experiment is shown in Fig. 8. The OH mole fraction is less almost by an order to that of water mole fraction. Though there is a slight over prediction at the first location ($X/D=10.8$ or 25.4mm), there is a good agreement between predicted OH mole fraction profiles with experiment in other locations. Rather good agreement in mixing layer that of core region is found at all locations. Figure 9 shows the quantitative comparison of computed water mole fraction profiles with experiment. The species production rates in the mixing region are well agreeing with experimental values. The water mole fraction values at core region could not be established exactly. Comparison of predicted

temperature profiles with experiment is given in Fig. 10. The predicted values of temperature in mixing layers and in core region have got appreciable agreement with that of experiment. The prediction capability of the code developed is proven by this comparison. In general the non-interference of fuel core to the outer region can be noticed in these plots.

4.3 Combustion of hydrogen the wake region of a strut

The two-dimensional numerical simulation of the flow field generated by the injection of a sonic stream of hydrogen jet in to hot air stream has been performed. The geometry used for the present analysis is similar to that proposed by Wepler and Koschel [11] and is shown in Fig.11. The wake region formed due to the wedge shaped strut enhances the mixing of the upcoming hydrogen jet. In addition to this reflected oblique shocks and its reflections from upper and lower walls along with the expansion wave from the lip of the strut interact with this wake region and the jet in its core. This lead to the formation of localized low velocity regions blocking the progress of the jet and hence sustained reaction zones in its outer periphery. But on the other hand, the same phenomena lead to pressure loss, which decides the total available thrust at the nozzle exit of the engine.

For the present analysis the geometry was divided into 105600 control volumes. The flow conditions for free stream and hydrogen injection is summarized in Table 4. More grids are provided down stream of the strut to capture wake and the

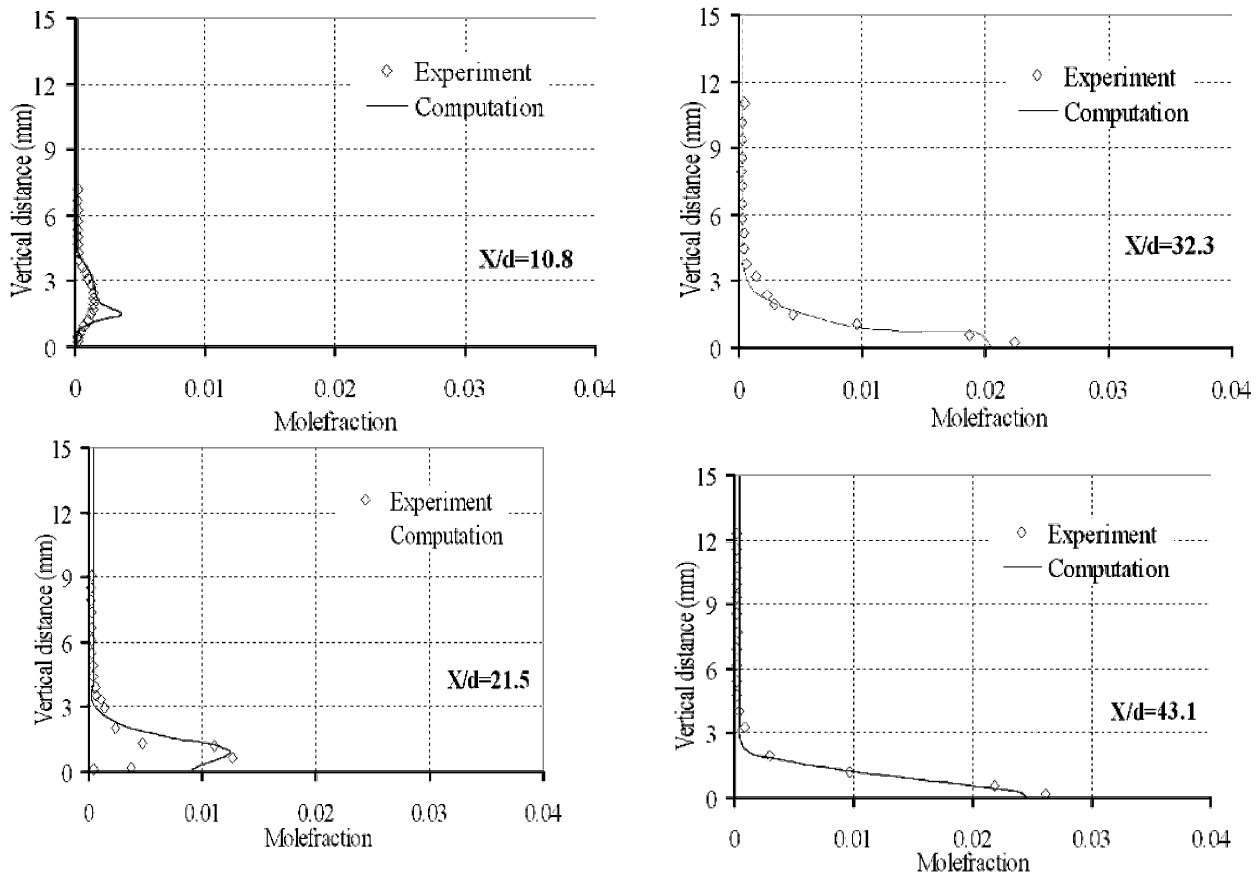


Fig.8 Comparison of predicted OH mole fraction profiles with experiment [7]

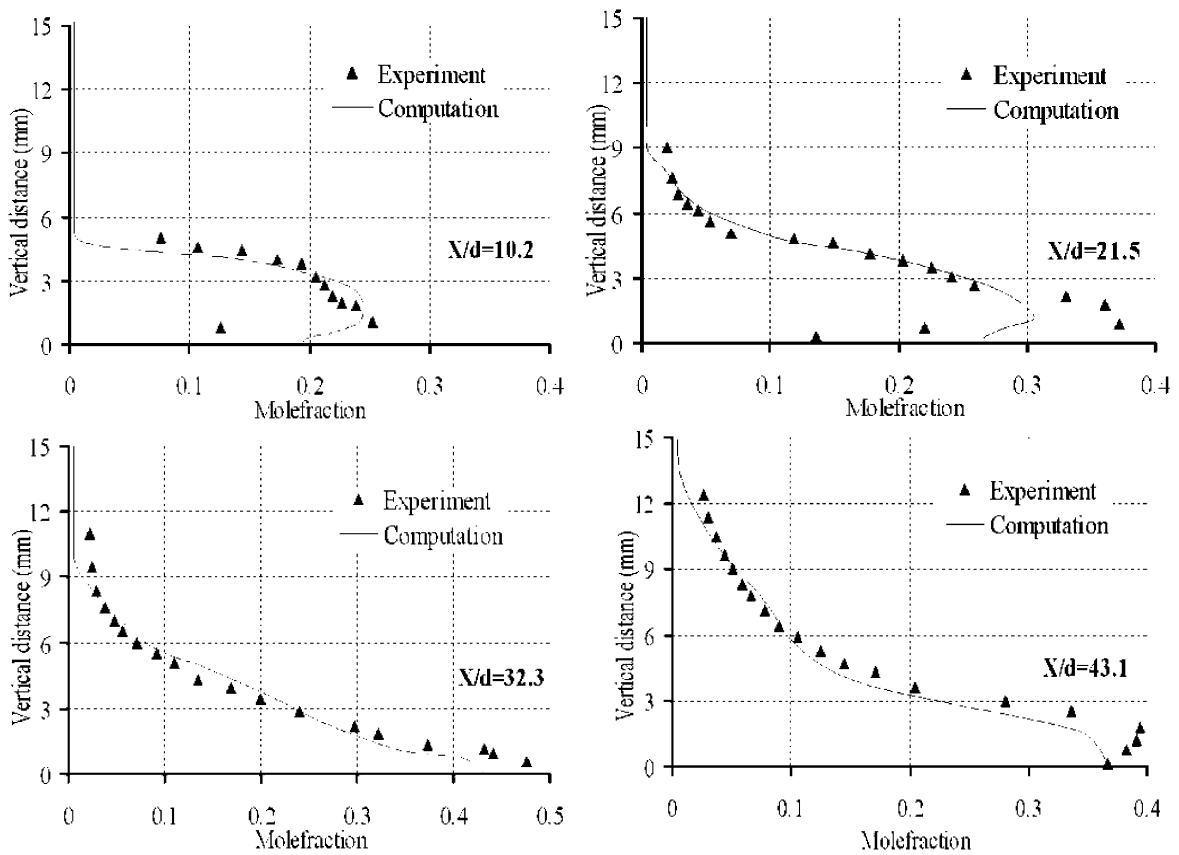


Fig.9 Comparison of predicted water mole fraction profiles with experiment [7]

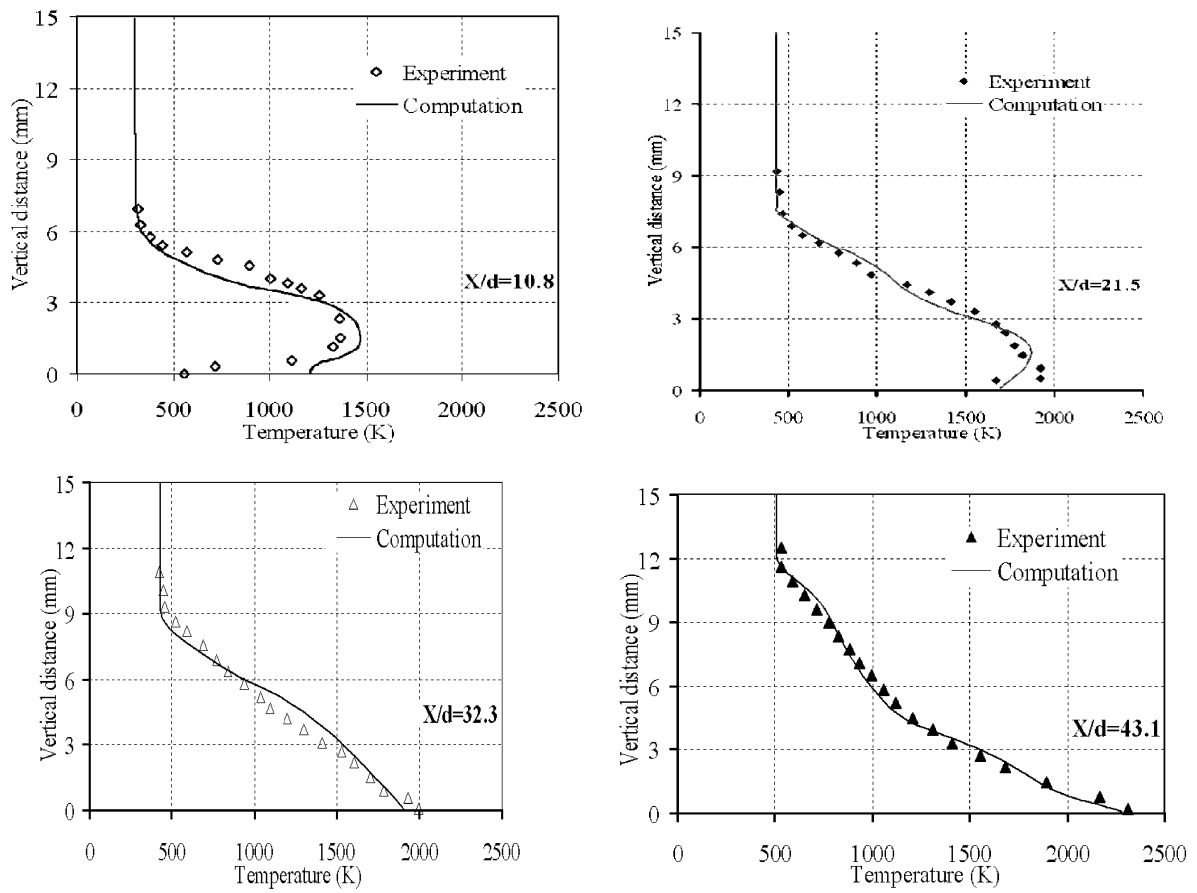


Fig.10 Comparison of predicted temperature profiles with experiment [7]

Table 4 Test conditions in strut injection

Free Stream Conditions	H ₂ Jet	Air Stream
Mach Number	1.0	2.47
Temperature, K	400.0	800
Pressure, Pa	121000	94000
H ₂ Mass Fraction	1.0	0
H ₂ O Mass Fraction	0	0
O ₂ Mass Fraction	0	0.23
N ₂ Mass Fraction	0	0.77

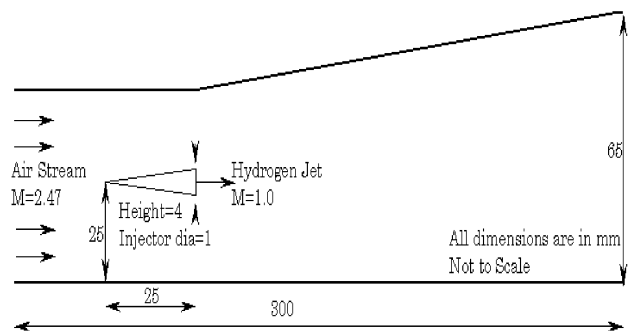


Fig.11 Schematic of the computational domain for wedge shaped strut injection

mixing structure.

The converged results (at CFL equal to 0.5) are post processed and the field view of Mach number is shown in Fig. 12. The oblique shock and its successive reflections are well captured. The alternate compression and expansion of the over expanded hydrogen jet and its interaction with shock reflection can be observed. Due to the effect of wake, localized recirculations zones with high residence time are created. There occurs sustained combustion and high temperatures in these areas can be

observed from field view of temperature (Fig. 13). The oblique shock originated from the leading edge of the strut creates an increase in temperature. This along with low velocity region in the lip initiates combustion. Further down stream the localized reaction pools generated due to shock/expansion wave interaction with wake-jet core system enhances mixing and reaction. Along the length of the combustor, the flame is found to be laterally spreading as the eddy systems grow in size. Water mole fraction plot shown in Fig. 14 also reveals the mixing enhancement and

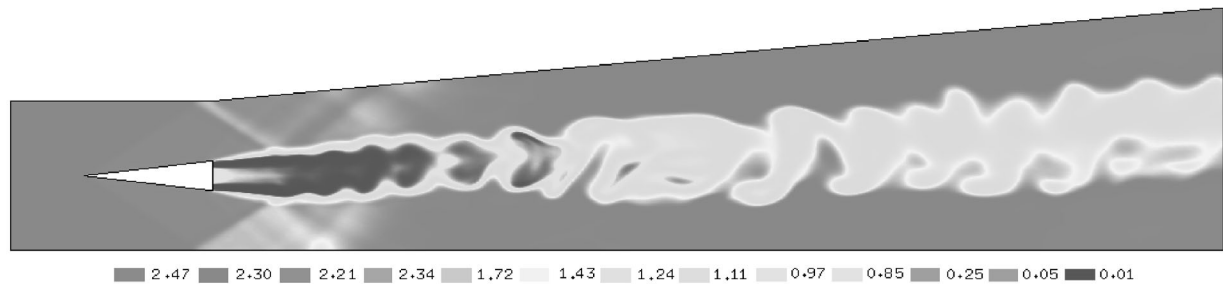


Fig.12 Field view of Mach number

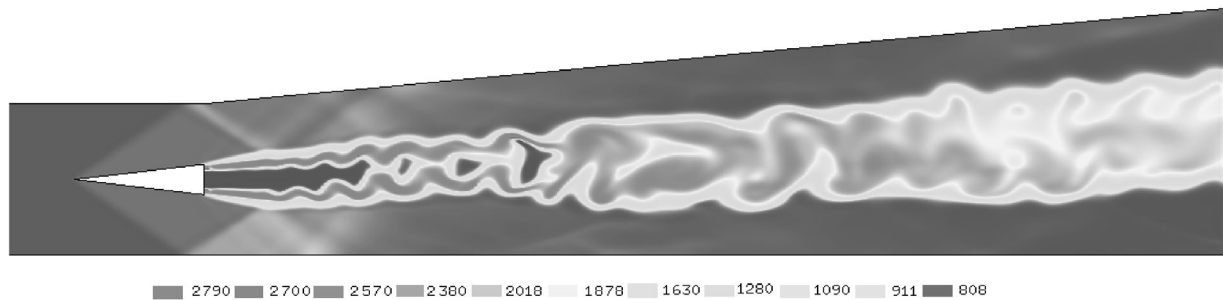


Fig.13 Field view of temperature

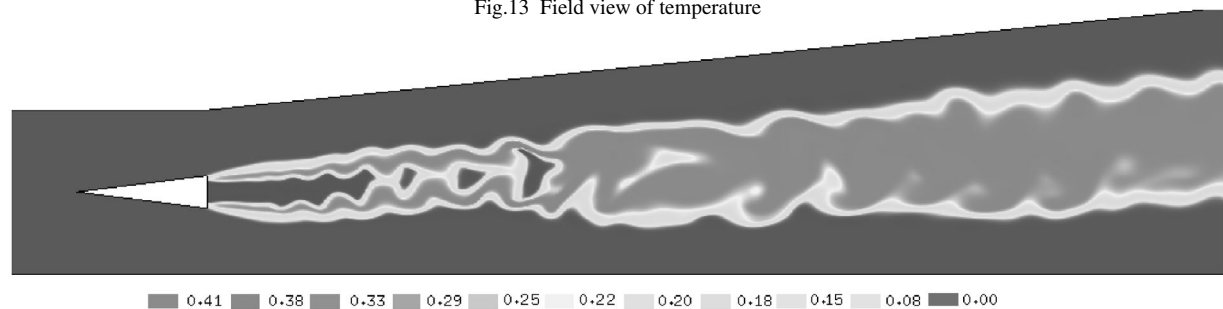


Fig.14 Field view of water mole fraction

reaction in wake jet interaction region.

Two sets of simulations with more pressure at inlet of the combustor for the free air stream (181500 Pa and 242000 Pa) have been performed, the convergence observed at the same higher CFL.

5. Conclusions

Computational analysis of supersonic turbulent reacting flow field has been performed with point implicit finite volume method on unstructured grids. The preconditioning used for chemical source terms has found to improve the capability of the code by increasing the CFL to 0.5, almost equal to that of the non-reacting version of the same code. The comparison of the computed data with experimental data has shown reasonable agreement. Simulation of the combustion of hydrogen injected to the wake region formed by a wedge shaped strut, revealed the enhancement of mixing and reaction in wake jet interaction region. Convergence at same CFL has been observed for tests with increased pressure at inlet for free stream air.

Though the reaction mechanism employed here is performing well when coupled with two-dimensional turbulent compressible Navier-Stokes equation; inclusion of more number of variables has created difficulties. It will set a real challenge, in terms of computer resources, while applying for scramjet combustors of larger geometry.

Acknowledgements

Authors thank T. Jayachandran, Head FMTD, VSSC, Thiruvananthapuram, India; for his valuable suggestions for the progress of this work.

References

1. Aso, S., Yamane, Y., and Kawano, S., *ISABE* 99-7141, (1999).
2. Aso, S., Tannou, M., Maekawa, S., and Fukuda, M, *AIAA Paper* 94-0707, (1994).
3. Mitani, T., Chizei, N., and Kanda, T., *AIAA Paper* 99-4871,

- (1999).
4. Evans, J. S., and Schexnayder, C. J., *AIAA Journal*, 18: 188-193 (1980).
 5. Bussing, T. R. A., and Murman, E. M., *AIAA Journal*, 26: 1070-1078 (1988).
 6. Burrows, M., C., and Kurkov, A., P., NASA TM X-2828 (1973).
 7. Cheng, T. S., Wehrmeyer, J. A., Pitz, R. W., Jarret, O., and Northam, J. B., *AIAA paper* 91-2320 (1991).
 8. Yakhot, V., Orzag, A., Gatski, T. B., and Speziade, C. B., *Physics of Fluids*, 4: 1510-1520 (1992).
 9. McBride, B. J., and Gordon, S., NASA SP-273 (1971).
 10. Baurle, R.A., and Girimaji, S. S., *AIAA Paper* 99-0928, (1999).
 11. Welper, U., and Koschel, W.,W., , *AIAA paper* 2002-3572, (2002).